PNAS RESEARCH ARTICLE | MEDICAL SCIENCES OPEN ACCESS

PGRN deficiency exacerbates, whereas a brain penetrant PGRN derivative protects, *GBA1* mutation-associated pathologies and diseases

Xiangli Zhao[a,1], Yi Lin[b,1], Benjamin Liou[b], Wenyu Fu[a], Jinlong Jian[a], Venette Fannin[b], Wujuan Zhang[c], Kenneth D. R. Setchell[c,d], Gregory A. Grabowski[b], Ying Sun[b,d,2], and Chuan-ju Liu[a,e,2]

Edited by Hugo Bellen, Baylor College of Medicine, Houston, TX; received June 16, 2022; accepted November 8, 2022

Mutations in *GBA1*, encoding glucocerebrosidase (GCase), cause Gaucher disease (GD) and are also genetic risks in developing Parkinson's disease (PD). Currently, the approved therapies are only effective for directly treating visceral symptoms, but not for primary neuronopathic involvement in GD (nGD). Progranulin (PGRN), encoded by *GRN*, is a novel modifier of GCase, but the impact of PGRN in *GBA1* mutation-associated pathologies in vivo remains unknown. Herein, $Grn^{-/-}$ mice crossed into $Gba^{9v/9v}$ mice, a *Gba1* mutant line homozygous for the *Gba1* D409V mutation, generating $Grn^{-/-}Gba^{9v/9v}$ (PG9V) mice. PG9V mice exhibited neurobehavioral deficits, early onset, and more severe GD phenotypes compared to $Grn^{-/-}$ and $Gba^{9v/9v}$ mice. Moreover, PG9V mice also displayed PD-like phenotype. Mechanistic analysis revealed that PGRN deficiency caused severe neuroinflammation with microgliosis and astrogliosis, along with impaired autophagy associated with the *Gba1* mutation. A PGRN-derived peptide, termed ND7, ameliorated the disease phenotype in GD patient fibroblasts ex vivo. Unexpectedly, ND7 penetrated the blood-brain barrier (BBB) and effectively ameliorated the nGD manifestations and PD pathology in $Gba^{9v/null}$ and PG9V mice. Collectively, this study not only provides the first line of in vivo but also ex vivo evidence demonstrating the crucial role of PGRN in *GBA1/Gba1* mutation-related pathologies, as well as a clinically relevant mouse model for mechanistic and potential therapeutics studies for nGD and PD. Importantly, a BBB penetrant PGRN-derived biologic was developed that may provide treatment for rare lysosomal storage diseases and common neurodegenerative disorders, particularly nGD and PD.

Gaucher disease | Parkinson's disease | progranulin | *GBA1* mutation | progranulin-derived biologic

Significance

This study carries immediate significance and novelty from following perspectives: (a) It provides the first line of in vivo and ex vivo evidence demonstrating the crucial role of PGRN in *GBA1* mutation-related diseases (i.e., GD and PD) and advances our understanding about the pathogenesis of GD and probably PD as well. (b) It also presents a clinically relevant mouse model for mechanistic and potential therapeutics studies for *GBA1* mutation-caused diseases, overcoming the barriers to allow the study in multiple organs in viscera and CNS. (c) Most excitingly, it develops a brain penetrant PGRN-derived biologics that protects against GD and PD-like pathologies, providing a potential treatment for rare lysosomal storage diseases and common neurodegenerative disorders, particularly nGD and PD.

Gaucher disease (GD), caused by *GBA1* mutations, is one of the most common lysosomal storage diseases (LSDs). *GBA1* encodes the lysosomal enzyme, glucocerebrosidase (GCase, EC 3.1.2.45) that is responsible for degradation of its substrates, glucosylceramide (GluCer) and glucosylsphingosine (GluSph). Homo- or bi-allelic mutations in the *GBA1* cause defective GCase function in GD affecting multiple organs in viscera and central nervous system (CNS) (1, 2). Reduced GCase activity and the subsequent accumulation of toxic lipids substrates, GluCer and GluSph, lead to inflammation and neurodegeneration in GD variants (2, 3). Three GD phenotypes are delineated by the absence (GD type 1) or presence and progression (GD types 2 and 3) of early onset primary neurological involvement (2, 4). Current enzyme replacement therapy (ERT) and substrate reduction therapy (SRT) are highly effective treatments for visceral involvement but have no direct effects on the CNS manifestations of neuronopathic involvement in GD (nGD) (5–8); this presents an urgent, unmet need to develop alternative treatments for GD, specifically nGD.

Widely used animal models to mimic specific human *GBA1* mutation-associated disease are knock-in mouse models with human *GBA1* point mutations identified in human GD patients (9, 10). Unfortunately, these mice do not develop substantial substrate accumulation or inflammation to cause easily detectable disease phenotypes; their nGD phenotypes are very mild to unseen. Additional chronic nGD models carry *Gba1* mutations homozygous for V394L or D409H combined with partially deficient prosaposin (PS-NA), a precursor of saposins (A, B, C, and D), were developed into resultant 4L/PS-NA and 9H/PS-NA mice, respectively (11). These chronic nGD models develop inflammation in visceral organs and CNS and neurodegeneration. However, the deficiency of saposins in these models leads to complex glycosphingolipids accumulation that may cause non-GD phenotypes. Thus, there is an unmet need to develop preclinical animal model(s) that recapitulate the human disease mechanisms and phenotypes, particularly for nGD.

Progranulin (PGRN) is a ubiquitously expressed glycoprotein linked to a variety of physiological processes, including tissue repair, wound healing, tumorigenesis,

Author contributions: X.Z., Y.L., W.F., J.J., Y.S., and C.L. designed research; X.Z., Y.L., B.L., V.F., W.Z., and K.D.R.S. performed research; X.Z., Y.L., G.A.G., Y.S., and C.L. analyzed data; W.F. and J.J. assisted with the experimental design; V.F. generated and maintained mouse models; W.Z. and K.D.R.S. performed and analyzed glycosphingolipids by LC-MS/MS; G.A.G. edited the manuscript; and X.Z., Y.L., Y.S., and C.L. wrote the paper.

The authors declare no competing interest.

This article is a PNAS Direct Submission.

[1]X.Z. and Y.L. contributed equally to this work.

[2]To whom correspondence may be addressed. Email: Ying.Sun@cchmc.org or Chuanju.Liu@nyulangone.org.

This article contains supporting information online at https://www.pnas.org/lookup/suppl/doi:10.1073/pnas.2210442120/-/DCSupplemental.

Published December 27, 2022.

anti-inflammation, and autoimmunity (12–15). PGRN also functions as an important neurotrophic factor, and mutations of *GRN* (encoding PGRN) are directly related to frontotemporal dementia, Parkinson's disease (PD), and other neurological diseases (16–18). Accumulating evidence from several laboratories, including ours, has also revealed the associations between PGRN deficiency and LSDs, i.e., neuronal ceroid lipofuscinosis 11, GD, and Tay-Sachs disease (19–23). We first reported PGRN as a novel modifier of GCase by showing linkage of GCase to heat shock protein 70 (Hsp70) via the C-terminal domain of PGRN that was essential for the association of PGRN with GCase and Hsp70 (24).

GRN or *GBA1* mutations or deficiencies have been associated with various rare LSDs and common neurodegenerative disorders (25, 26). Besides GD, evidence indicates that *GBA1* mutations are also major genetic risk factors for developing PD, even in the heterozygous carrier state (18, 27). However, whether and how PGRN is functionally involved in *GBA1* mutation-associated pathologies and diseases in vivo remains unclear. Here, PGRN deficient mice ($Grn^{-/-}$) were crossed into $Gba^{D409V/D409V}$ ($Gba^{9v/9v}$) mice, which is a *Gba1* mutant line that is homozygous for the *Gba* D409V mutation, thereby generating the *Grn* and *Gba1* double mutant $Grn^{-/-}Gba^{9v/9v}$ (termed PG9V) mice. Comprehensive characterization of PG9V mice as well as mechanistic analyses identified the crucial role of PGRN in *GBA1* mutation-related pathologies. Also, an approximately 15-kDa biologic ND7, derived from PGRN C terminus, was shown to penetrate across the blood-brain barrier (BBB), enter the brain parenchyma, and, unexpectedly, demonstrate therapeutic potentials against nGD and probably PD.

Results

PG9V Mice Exhibited Hepatosplenomegaly and Behavioral Deficits. Ovalbumin-challenged and aged-$Grn^{-/-}$ mice displayed GD-like phenotypes in multiple organs (20, 28), and PGRN deficiency in GD patient fibroblasts potentiated a GD phenotype and autophagy defect (29); these indicated that PGRN deficiency modulates the severity of GD phenotypes. However, whether PGRN is important for *GBA1* mutation-associated pathologies and diseases in vivo remained largely unclear. To this end, we generated *Grn* and *Gba1* double mutant, PG9V mice, by crossing $Grn^{-/-}$ mice with $Gba^{9v/9v}$ mice (*SI Appendix*, Fig. S1*A*). Genotyping and real-time PCR were used to identify and confirm the PG9V mice genotype (*SI Appendix*, Fig. S1 *B* and *C*). Both male and female PG9V mice were fertile and had about an 18-mo's life span. Increased ratio of spleen or liver per body weight, suggesting hepatosplenomegaly, a typical feature of GD, was observed in 8-mo-old PG9V mice compared to age-matched $Grn^{-/-}$ and $Gba^{9v/9v}$ mice (Fig. 1*A*) and was age-dependent (Fig. 1*B*).

Since PG9V mice developed early onset and progression of hepatosplenomegaly, the footprint patterns of the four genotype mice were assessed at 8 mo of age to detect gait abnormalities, a general indicator of disease locomotor progression. The gait of $Gba^{9v/9v}$ and $Grn^{-/-}$ was comparable to those in WT mice with similar spaced strides and overlapping placement of footprint. In contrast, PG9V mice have a shortened stride with a pronounced splaying of the rear limbs as indicated by the shortened stride length and wider hind base as well as bigger spaces of overlapping (Fig. 1 *C* and *D*). PG9V mice also showed hind limb clasping during tail hanging by the ages of 12 mo and 18 mo; the 18-mo-old PG9V mice developed a kyphotic posturing, similar to that found in some nGD patients, and exhibited severe hind limb paresis. Gait ataxia was also present, which mimics signs in some neurodegenerative GD type 3 patients (2, 3). In comparison, $Gba^{9v/9v}$, $Grn^{-/-}$, and WT mice at the age of 12 mo did not display any of these behavioral deficits (Fig. 1*E*). These observations indicated that loss of PGRN in $Gba^{9v/9v}$ mice was required for the development of neurologic phenotypes.

PGRN Deficiency in *Gba1* Mutant Mice Potentiated GD Storage Cells and Lysosomal Abnormality. Presence of enlarged macrophages or storage cells (Gaucher cells, GD cells) is a typical GD pathology. The numbers of GD cells were significantly increased in the liver, lung, and spleen of PG9V mice compared to $Gba^{9v/9v}$ and $Grn^{-/-}$ mice at 12 mo of age (Fig. 2 *A* and *B*). Additionally, GD cells were also detected in liver, lung, and spleen of PG9V mice as early as at 8 mo of age (*SI Appendix*, Fig. S2). Transmission electron microscopes (TEM) revealed that a large number of tubular-like lysosomes were present in lung tissues from 18-mo-old PG9V mice, while very few were detected in $Grn^{-/-}$ mice and were non-detectable in $Gba^{9v/9v}$ and WT mice (Fig. 2 *C* and *D*). Additional analysis demonstrated that these tubular-like lysosomes were observed mostly in lung macrophages of PG9V mice (*SI Appendix*, Fig. S3). Furthermore, the lysosomes were examined in the brain tissues of WT, $Gba^{9v/9v}$, $Grn^{-/-}$, and PG9V mice using immunofluorescence staining with antibody against LAMP2, a lysosomal membrane protein. Higher densities of LAMP2-positive vacuoles were frequently present in the brain sections of 12-mo-old PG9V mice, as compared to those in the mice with other genotypes (Fig. 2 *E* and *F*).

PG9V Mice Exaggerated GCase Activity Reduction and Substrate Accumulation. The observed GD cells and abnormal lysosomes in PG9V mice prompted us to examine the GCase activity and the levels of its substrates, GluCer and GluSph, in these mice, using 4MU-Glc substrates (Fig. 3*A*) and liquid chromatography with tandem mass spectrometry (LC-MS/MS) (Fig. 3*D*), respectively. Loss of PGRN ($Grn^{-/-}$) resulted in reduction of GCase activities in liver and brain in $Grn^{-/-}$ mice with normal *Gba1* compared to that in age-matched WT mice at 1- and 8-mo of age (Fig. 3 *B* and *C*). Of note, GCase activities in liver and brain of 8-mo-old mice displayed similar pattern and close mean values as those in 1-mo-old mice (Fig. 3 *B* and *C*), indicating that GCase activity did not show age-dependent change and was consistent among juvenile (1 mo) and aged (8 m) PG9V mice and other genotypes. Additionally, PGRN deficiency reduced the GCase activity in liver, spleen, and brain, but not in lung in $Grn^{-/-}$ mice, suggesting the effects of PGRN deficiency on GCase activity appeared to be tissue-specific (Fig. 3 *B* and *C* and *SI Appendix*, Fig. S4). Although the loss of PGRN ($Grn^{-/-}$) resulted in reductions of GCase activities in liver and brain compared to age-matched WT mice, this was not observed in the very low activity in PG9V mice at 1 and 8 mo old compared to $Gba^{9v/9v}$ (Fig. 3 *B* and *C* and *SI Appendix*, Fig. S4).

Since 4MU-Glc assays measure total cellular GCase activity, this could be due to diminished trafficking of 9V GCase and would not accurately reflect the lysosomal GCase activity levels. Thus, we relied on quantification of GluCer and GluSph levels by LC-MS/MS (Fig. 3*D*), which do reflect lysosomal GCase activity. Massive accumulations of GluCer were present in PG9V vs. other genotypes (Fig. 3 *F* and *G*). In liver and lung tissues, neither the loss of PGRN ($Grn^{-/-}$) nor the presence of a *Gba1* mutation ($Gba^{9v/9v}$) significantly altered GluCer levels compared to that in age-matched WT (Fig. 3 *E* and *F*, *Upper*). However, PG9V mice demonstrated dramatically increased GluCer levels in liver (16.9-fold vs. WT; 12.3-fold vs. $Grn^{-/-}$; 5.6-fold vs. $Gba^{9v/9v}$) and lung (18.2-fold vs. WT; 18.2-fold vs. $Grn^{-/-}$; 9.5-fold vs. $Gba^{9v/9v}$) (Fig. 3 *E* and *F*, *Upper*). Of note, the mean GluCer level in midbrain of $Gba^{9v/9v}$ mice was higher than that in WT mice, but not reached to significance by one-way ANOVA analysis ($P = 0.3475$). In PG9V mice, loss of PGRN in $Gba^{9v/9v}$ resulted in significantly elevated GluCer levels in midbrain than those in WT, $Grn^{-/-}$, and $Gba^{9v/9v}$ control mice (Fig. 3 *E–G*, *Upper*).

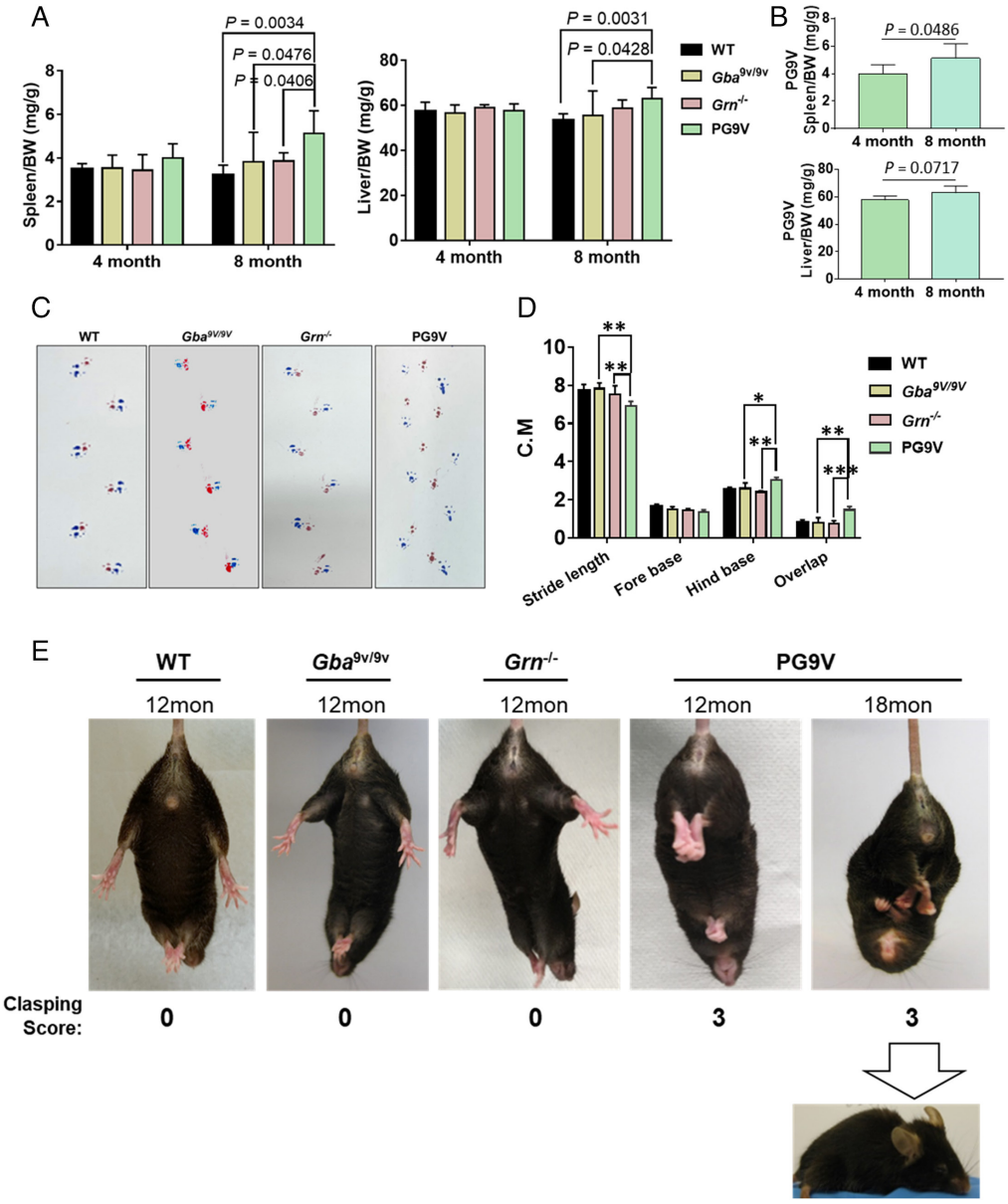

Fig. 1. PG9V mice exhibited hepatosplenomegaly and behavioral deficits. (*A*) PG9V mice developed hepatosplenomegaly. Spleen and liver weight divided by total animal body weight were graphed for 4-mo- and 8-mo-old WT, *Gba*$^{9v/9v}$, *Grn*$^{-/-}$, and PG9V mice. (*B*) Age dependence of hepatosplenomegaly in PG9V mice. The ratio of spleen/body weight or liver/body weight between 4-mo- and 8-mo-old PG9V mice was compared. (*C*) Gait analysis. The footprint patterns in *C* of 8-mo-old WT, *Gba*$^{9v/9v}$, *Grn*$^{-/-}$, and PG9V mice, $n = 5$ to 8. (*D*) The footprint patterns were quantified by four measurements: stride length, front base width, hind base width, and front/hind footprint overlap. (*E*) Hind limb clasping test. PG9V showed hind limb clasping at 12 mo of age with test score of 3 (0 to 3, 0 = normal). The age-matched WT, *Gba*$^{9v/9v}$, and *Grn*$^{-/-}$ mice displayed no clasping with a score of 0. PG9V at 18 mo showed kyphosis posture. One-way ANOVA test for (*A*), and *t* test for (*B*). $n = 5$ to 8 mice per group.

GluSph, secondary substrate of GCase (GluCer as primary), was also massively increased in PG9V lung and brain vs. the other genotypes (Fig. 3 *G* and *F*, *Bottom*). GluSph shows minor increases in PG9V relative to *Gba*$^{9v/9v}$ in liver (Fig. 3 *E*, *Bottom*). Progressive accumulation of substrates was studied in lung tissues. Both GluCer and GluSph in lung tissues of PG9V mice at ages of 4, 8, and 12-mo exhibited consistently higher and gradually increased levels than those in control groups (*SI Appendix*, Fig. S5). Intriguingly, unlike GluCer, GluSph levels in lung and brain of *Gba*$^{9v/9v}$ were all significantly higher than WT (Fig. 3 *E–G*, *Bottom*), suggesting the residual enzymatic activity in *Gba*$^{9v/9v}$ was sufficient to prevent the accumulation of GluCer but not the neurotoxic lipid, GluSph that has much lower catalytic rate constant compared to GluCer, therefore requires much more GCase for its lysosomal degradation (30). In addition, the distribution of accumulated GluCer in brain tissues was assessed by immunofluorescence staining using anti-GluCer antibody (*SI Appendix*, Fig. S6). *Grn*$^{-/-}$ and *Gba*$^{9v/9v}$ mice showed increased GluCer positive signals in the hippocampus, cortex, and midbrain tissues compared with WT mice, and the positive signal of GluCer was further enhanced in PG9V mice compared with *Grn*$^{-/-}$ and *Gba*$^{9v/9v}$ mice (*SI Appendix*, Fig. S6). Taken together, these results demonstrated that deletion of PGRN in *Gba*$^{9v/9v}$ mice impaired GCase catalytical function, leading to enhanced substrate accumulations.

PG9V Mice Displayed Neuropathic Phenotypes, Including PD-Like Signs. PGRN mutation and deficiency were reported to be associated with various neurodegenerative diseases, including Alzheimer's disease (AD) and PD (31–33). In neurodegenerative diseases, the accumulations of many disease-pathogenic protein aggregates

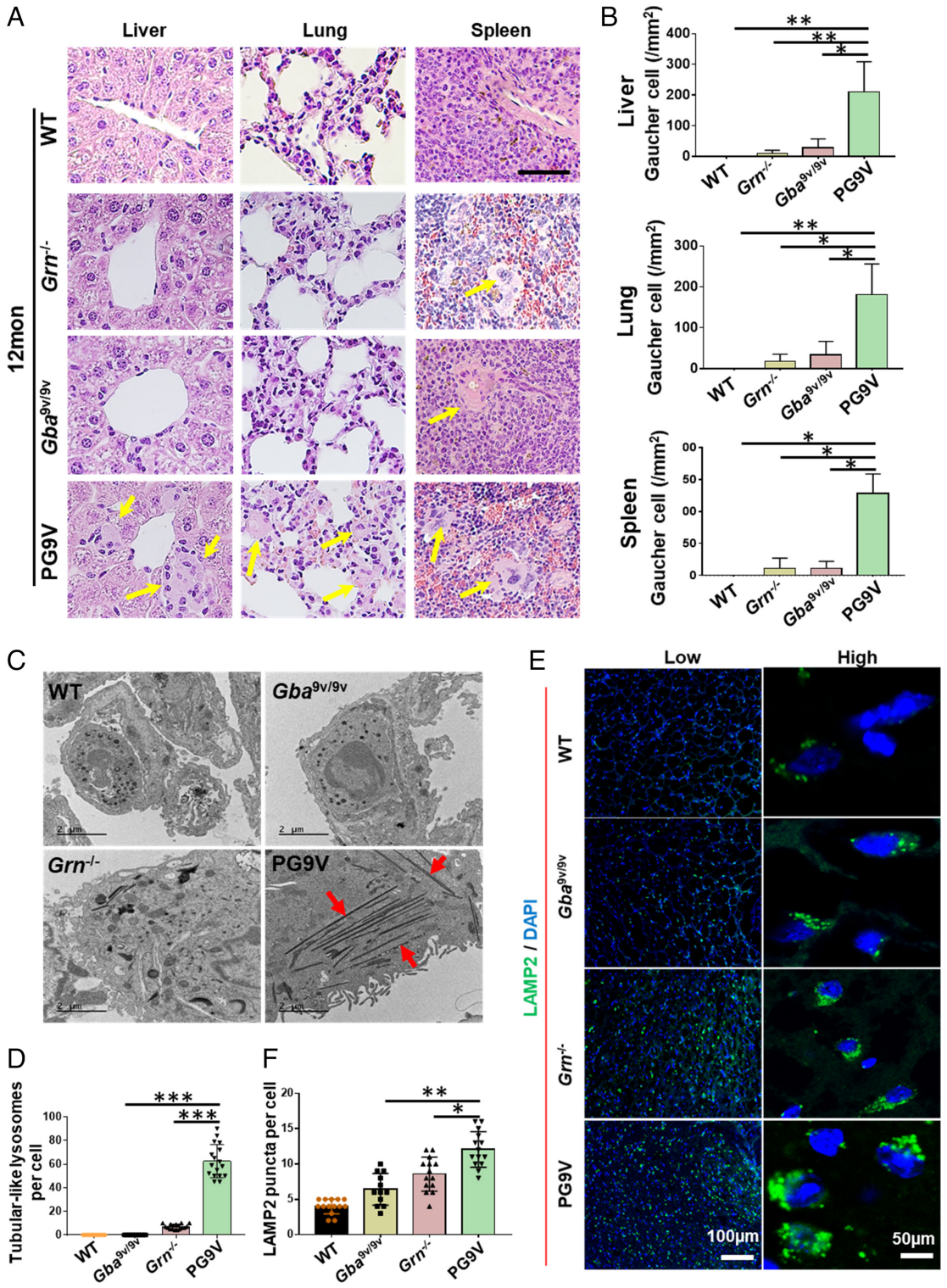

Fig. 2. PGRN deficiency potentiated GD storage cells in *Gba1* mutant mice. (*A*) Storage cells in PG9V mice. Tissue sections were stained by H&E. Yellow arrow indicates the large storage cells. (Scale bar, 50 μM for all images.) (*B*) Quantification of storage cells in *A*. (*C*) Typical tubular-like lysosomes (indicated by the red arrow) were found in 18-mo-old lung tissue in PG9V mice under TEM. (*D*) Quantification of tubular-like lysosomes in *C*. (*E*) Immunofluorescence staining of LAMP2 (green) in 12-mo-old brain tissue of WT, $Gba^{9v/9v}$, $Grn^{-/-}$, and PG9V mice. DAPI stained cell nuclei. (*F*) Quantification of LAMP2-positive cells in *E*. Data are shown as mean ± SD. One-way ANOVA tests. **P* < 0.05; ***P* < 0.01; ****P* < 0.001.

were reported to be commonly implicated in brain. These include β-Amyloid and Tau in AD and frontotemporal disorders (FTD), α-Syn in PD and multiple system atrophy, and TAR DNA-binding protein 43 (TDP-43) in FTD and amyotrophic lateral sclerosis (34, 35). Both in PG9V and $Grn^{-/-}$ mice, we observed significantly enhanced expression of phosphorylated α-Syn (PS-129), which was implicated in the pathogenesis of PD (36), and β-Amyloid compared to wildtype (WT) and $Gba^{9v/9v}$ mice (Fig. 4 *A* and *B*). Importantly, PG9V mice demonstrated significant higher levels of α-Syn and β-Amyloid than those in $Grn^{-/-}$ mice (Fig. 4 *A* and *B*). In addition, PG9V and $Grn^{-/-}$ mice also exhibited significantly higher Tau (Fig. 4*C*) and TDP-43 (*SI Appendix*, Fig. S7) aggregates

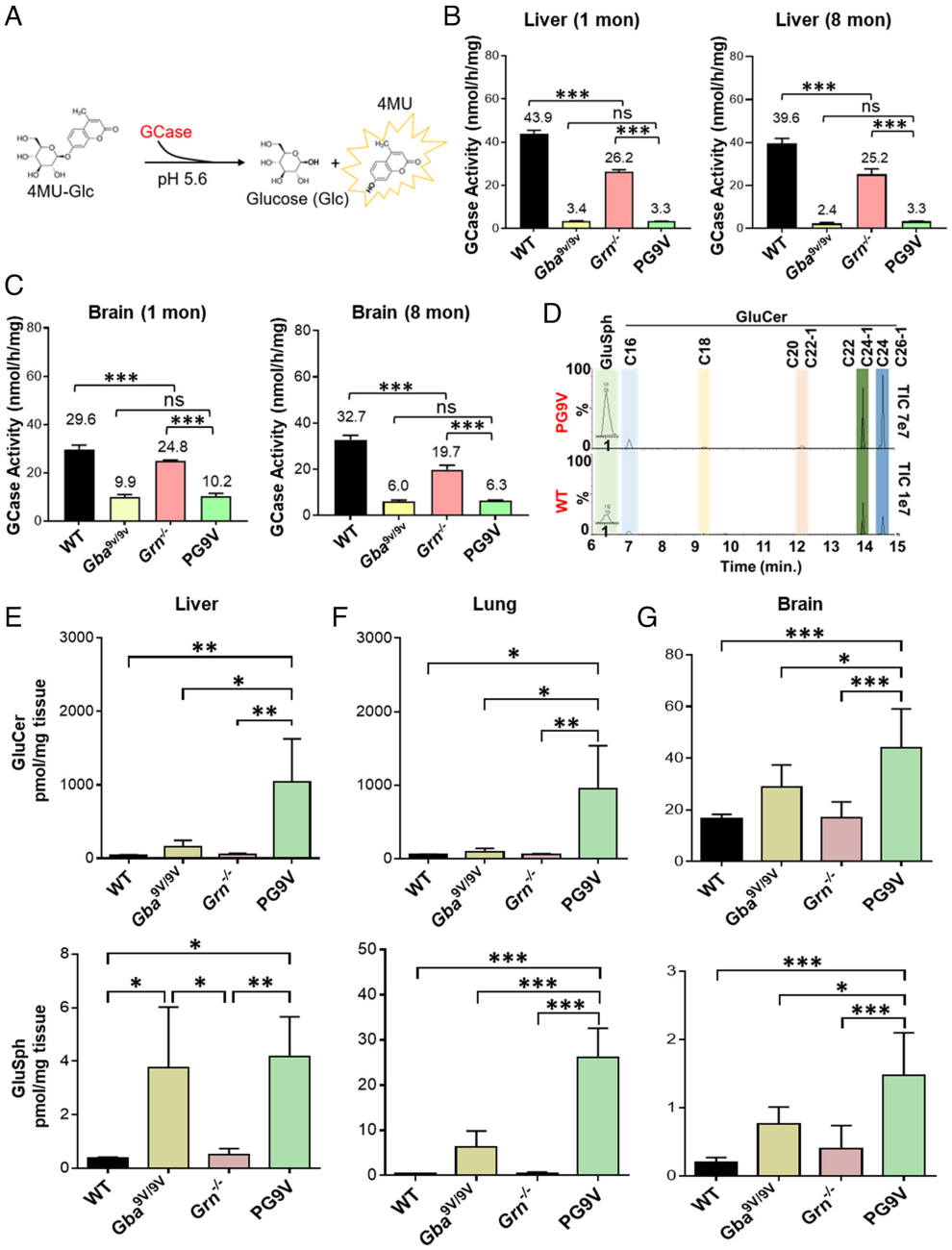

Fig. 3. PG9V mice exaggerated GCase activity reduction and substrate accumulation. (*A*) Schematic of GCase activity reaction. (*B* and *C*) GCase activity was determined fluorometrically using 4MU-Glc as substrate in liver (*B*) and brain (*C*) collected from 1- and 8-mo-old WT, $Grn^{-/-}$, $Gba^{9v/9v}$, and PG9V mice. (*D*) Schematic of glycosphingolipids quantification by LC-MS/MS. (*E*–*G*) Substrate levels of glucosylceramide (GluCer) and glucosylsphingosine (GluSph) in liver (*E*), lung (*F*), and midbrain (*G*) from 8-mo-old WT, $Grn^{-/-}$, $Gba^{9v/9v}$, and PG9V mice analyzed by LC-MS/MS. Data are shown as mean ± SD. $n = 5$ to 10. One-way ANOVA tests. *$P < 0.05$; **$P < 0.01$; ***$P < 0.005$.

in cortex, midbrain, and hippocampus than WT and $Gba^{9v/9v}$ mice. Moreover, the midbrain region of PG9V showed significantly higher level of Tau/ TDP-43 aggregates than that in $Grn^{-/-}$ mice (Fig. 4*C* and *SI Appendix*, Fig. S7). These data indicated that PG9V mice at 12 mo and older developed neurodegenerative phenotypes that are found in nGD and PD patients (37, 38), but these phenotypes were undetectable in $Gba^{9v/9v}$ mice or at moderate level in $Grn^{-/-}$ mice. Thus, this double mutant PG9V model provides a clinical-relevant model system for pathophysiological studies and for testing therapeutic approaches for GD and PD.

PGRN Deficiency Potentiated Macrophage Activation, Microgliosis, and Astrogliosis in *Gba1* Mutant Mice. Chronic inflammation and dysregulated immune cells, particularly macrophages, play critical roles in the pathogenesis of GD (22, 39). PGRN deficiency leads to enhanced inflammation through activating macrophages (40), suggesting that macrophage activation may be one of the underlying molecular mechanisms involved in the visceral organs and CNS manifestations in PG9V mice. Immunohistochemistry staining revealed that the signals of CD68, an activated macrophage and microglia marker, were markedly stronger in PG9V mice than those in $Grn^{-/-}$, $Gba^{9v/9v}$, and WT controls in various tissues tested (about 100-fold in PG9V than those in other controls), including in brain and spinal cord as well as in liver, lung, and spleen (Fig. 5 *A*–*C*).

Microglia are the CNS resident macrophages and act as the first and main form of active immune defense in the CNS. Activation of microglia (microgliosis) is a typical indicator of neuroinflammation (41). To further determine the microglia pathology in CNS, Iba1

and TMEM119, two markers for activated microglia (42, 43), were tested on the brain sections from 12-mo-old WT, *Gba*$^{9v/9v}$, *Grn*$^{-/-}$, and PG9V mice by immunofluorescence staining. Enhanced fluorescence signals in Iba1$^+$ and TMEM119$^+$ cells were observed in midbrain, cerebellum, and cortex from *Grn*$^{-/-}$ mice compared to that in WT and *Gba*$^{9v/9v}$ mice, which were maintained in baseline level (*SI Appendix*, Figs. S8 and S9). In the brain of PG9V mice, the signals of Iba1 and TMEM119 were both strongly increased in the midbrain, cortex, and cerebellum in comparison with WT, *Gba*$^{9v/9v}$, and *Grn*$^{-/-}$ mice, suggesting enhanced microgliosis in PG9V mice (*SI Appendix*, Figs. S8 *A* and *B* and S9). These immunofluorescence staining results were further confirmed by western blot analysis using antibody against Iba1 in brain lysates (*SI Appendix*, Fig. 8 *C* and *D*).

Astrogliosis with presence of reactive astrocytes in brain is another pathological indicator of neurodegenerative diseases (44, 45). PG9V mice exhibited markedly enhanced glial fibrillary acidic protein (GFAP) expression in various brain regions compared to *Grn*$^{-/-}$, *Gba*$^{9v/9v}$, and WT mice (Fig. 5*D*). Specifically, the GFAP signals in the thalamus (Th), brainstem (Bs), midbrain (Mb), and cortex (Ctx) of the PG9V brains were significantly stronger than those in other controls (Fig. 5 *D*–*F*). In addition, astrocytes in brain of PG9V mice displayed enlarged hypertrophic cell bodies with more astrocytic ramified filaments (*Insets* in Fig. 5*E*). Western blotting of GFAP in brain lysates confirmed that PGRN deficiency increased the GFAP protein levels in PG9V mice (*SI Appendix*, Fig. S8 *C* and *D*).

Deletion of PGRN Enhanced M1 and Inhibited M2 Macrophage Polarization. Phenotypes of macrophages can be predominantly separated into two major categories: pro-inflammatory M1 and anti-inflammatory M2. The imbalance of these two macrophage types is involved in numerous inflammation- and immunity-related diseases (46). The differential polarization of macrophage subtypes is a multifactorial process in which multiple regulators are involved (47). Recently, PGRN was reported as one of these factors to regulate macrophage polarization (48, 49). Since PGRN deficiency enhanced the macrophage/microglial activation in PG9V mice, macrophage polarization was then analyzed in 12-mo-old mice brain tissues. By immunofluorescence staining, M1 and M2 macrophages were identified by F4/80 and iNos (F4/80$^+$iNos$^+$), and F4/80 and CD206 (F4/80$^+$CD206$^+$), respectively. Both PG9V and *Grn*$^{-/-}$ mice had more M1 macrophages (F4/80$^+$iNos$^+$ ratio in all F4/80$^+$ macrophage) but less M2 macrophages (F4/80$^+$CD206$^+$ ratio in all F4/80$^+$ macrophage) compared to WT and *Gba*$^{9v/9v}$ mice (*SI Appendix*, Fig. S10 *A*–*D*). However, the ratio of M1 and M2 macrophages was not significantly differential between WT and *Gba*$^{9v/9v}$ mice. Taken together, the imbalanced macrophage polarization caused by PGRN deficiency may contribute to the acute inflammation seen in PG9V mice.

PGRN Deficiency Led to the Autophagic Vacuoles Accumulation and Lipofuscin Aggregation. PGRN deficiency increases the autophagy marker LC3-II in the brain of aged mice (40) as well as activates the autophagy pathway that is mediated by autophagosome-lysosome fusion (29). Next, we explored if PGRN deficiency affected autophagy in *Gba1* mutant mice. Autophagy markers LC3-II and p62 in the brains of PG9V mice were found significantly elevated compared to *Grn*$^{-/-}$ or *Gba*$^{9v/9v}$ controls (*SI Appendix*, Fig. S11 *A* and *B*). Autophagic vacuoles are much fewer in vivo in the intact mature brain in normal condition (50). Under TEM, more autophagic vacuoles (red arrows) were observed in the brain tissue of PG9V mice compared with those in *Grn*$^{-/-}$, *Gba*$^{9v/9v}$, and WT mice (*SI Appendix*, Fig. S11*D*). These findings revealed that the loss of PGRN exacerbated impaired autophagy in *Gba1* mutant mice, which may contribute to the development of neurological phenotypes observed in PG9V mice.

Age is one of the risk factors for various neurodegenerative diseases (51), and PGRN was reported to play an important role in maintaining neuronal function during aging (28). In CNS, one of the most striking morphologic changes in neurons during aging is the presence of lipofuscin aggregates (52). In brain of the 18-mo-old PG9V and control mice, substantial accumulation of lipofuscin granules shown as more and darker areas (red arrow) in TEM images was observed than that in other control mice (*SI Appendix*, Fig. S12). Together, PGRN deficiency plays pivotal roles in promoting CNS autophagosomes accumulation and lipofuscin aggregation that could contribute to behavioral deficits, GD, and PD-like phenotypes in PG9V mice.

PGRN Derivative ND7 Could Penetrate BBB and Benefit CNS. Previously, we showed therapeutic effects of PGRN protein in mitigating GD phenotypes (24). However, there is a concern of potential side effect of long-term usage of PGRN due to its potential oncogenic activity (13, 53). Therefore, a C-terminal 98 amino acid fragment of PGRN, named ND7, which retains the GCase binding and therapeutic activity of PGRN but lacks its oncogenic action, was developed (Fig. 6*A*) (24). To evaluate if ND7 can be served as a therapeutic against disease progression in GD mouse models, we expressed and purified the recombinant His-tagged ND7 peptide. Purity of ND7 was analyzed by Coomassie blue staining and western blotting with anti-PGRN antibody (Fig. 6*B*). The short-term efficacy of ND7 was first evaluated in *Gba*$^{9v/null}$ mice, which carries D409V mutation and the *Gba1* knockout (null) in another allele. *Gba*$^{9v/null}$ mice have reduced residual GCase activity (<5% of WT) than that of *Gba*$^{9v/9v}$ mice (9). After one dose of His-tagged ND7 (16 mg/kg body weight) administrated by intraperitoneal (IP) injection in 2-mo-old *Gba*$^{9v/null}$ mice, ND7 was widely detected in visceral organs (lung, liver, and spleen) at 30 min post-injection using anti-His-tag antibody (Fig. 6*C*). Unexpectedly, ND7 was also found in several brain regions, including cortex, cerebellum, and hippocampus with more intensive positive signals than that in the visceral organs (Fig. 6*C*). In vehicle (phosphate-buffered saline (PBS)) injected *Gba*$^{9v/null}$ mice, ND7 conjugated His-tag signal was barely detectable in corresponding tissues (*SI Appendix*, Fig. S13*A*). Accordingly, compared to vehicle control (0 h), GCase activity was significantly increased in the liver and brain in ND7-treated mice at 0.5 to 2 h after injection (*SI Appendix*, Fig. S13*B*). This data suggested that ND7 could efficiently cross the BBB, penetrate into brain tissues, and enhance brain GCase activity. To explore if activation of GCase is ND7 dose-dependent, *Gba*$^{9v/null}$ mice received weekly IP injection of 1, 4, or 16 mg ND7/kg for 4 wk. Interestingly, all three doses of ND7 increased the GCase activity in lung and spleen, but not in a dose-dependent manner (*SI Appendix*, Fig. S13*C*). Therefore, 1 mg/kg was selected for treatment in PG9V model.

Next, the long-term anti-GD therapeutic efficacy of ND7 was evaluated in the PG9V mice model, and ND7 was administrated by IP injection to 10-mo-old PG9V mice with a dose of 1 mg/kg body weight, three times per week, and lasted for 2 mo. PBS and imiglucerase (2.5 U/kg body weight), an Food and Drug Administration (FDA) approved recombinant GCase used as enzyme replacement drug for type 1 GD, served as controls. Compared to PBS control, both ND7 and imiglucerase increased the GCase activity in the liver of PG9V mice (Fig. 6*D*). However, only ND7 treatment significantly increased GCase activity in the brain tissue (Fig. 6*D*). As expected, imiglucerase treatment did not significantly alter the GCase activity in brain, which was comparable to PBS treated group as recombinant GCase enzyme cannot penetrate the BBB (Fig. 6*D*). Accordingly, ND7 treatment decreased the accumulation of GluCer, the primary and direct substrate of GCase, in the brain tissue compared to PBS and

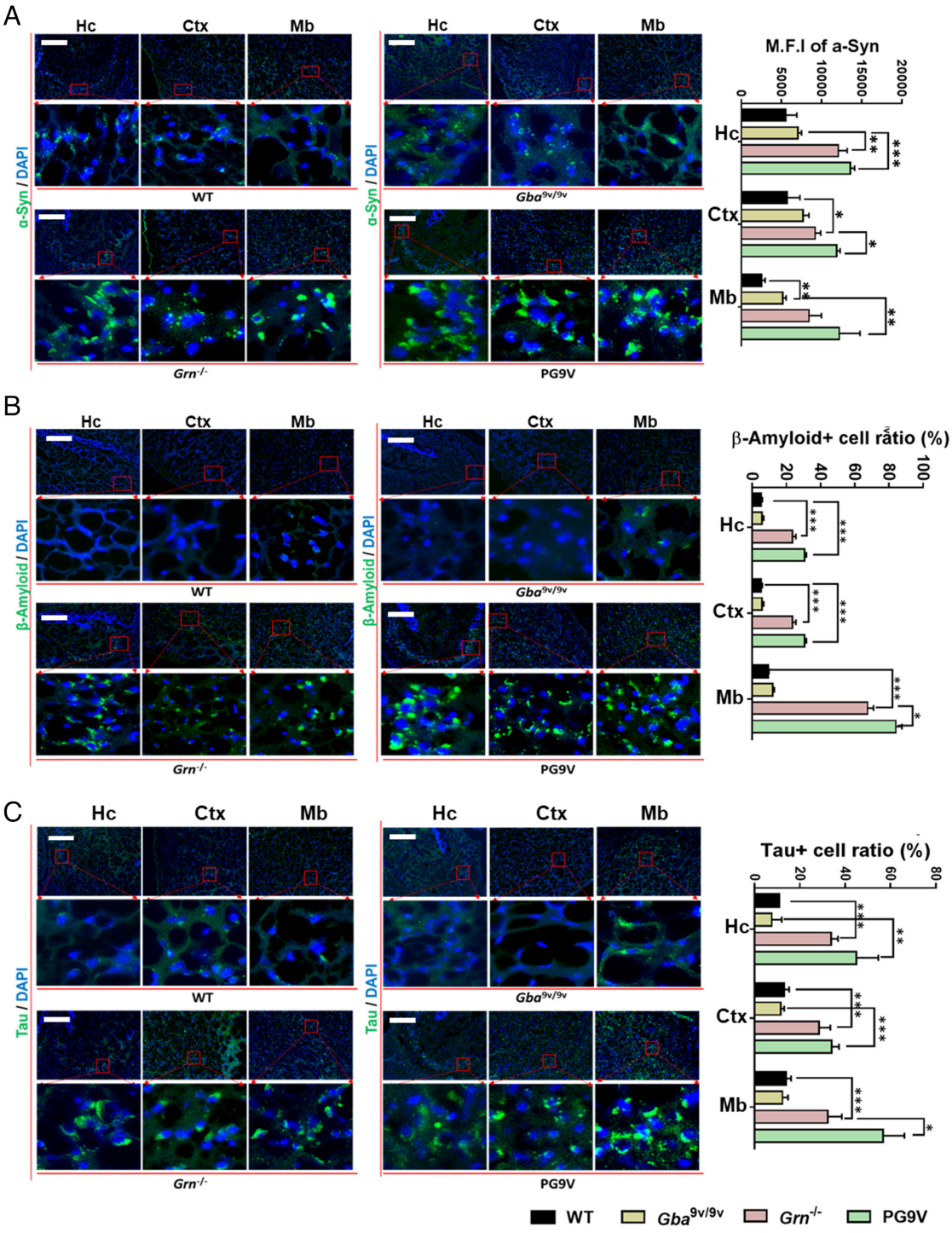

Fig. 4. Enhanced accumulation of α-Syn, β-Amyloid, and Tau in the brain tissues of PG9V mice. Immunofluorescence staining in the brains of 12-m-old WT, $Gba^{9v/9v}$, $Grn^{-/-}$, and PG9V mice for (*A*) α-Syn (green), (*B*) β-Amyloid (green), and (*C*) Tau (green) with corresponding quantification analysis showing in the graphs. *Insets* (red boxes) in *A–C* are zoomed-in and shown in the *Lower* panel. DAPI stained cell nuclei. Hc, hippocampus; Ctx, cortex; Mb, midbrain. (Scale bar, 100 μM.) Data are shown as mean ± SD. One-way ANOVA test. *$P < 0.05$; **$P < 0.01$; ***$P < 0.005$.

imiglucerase-treated PG9V mice (Fig. 6 *E* and *F*). Furthermore, ND7-treated mice were explored for alleviation of tissue inflammation. Both ND7 and imiglucerase markedly reduced the macrophage activation in lung and liver (*SI Appendix*, Fig. S14 *A* and *B*). Most importantly, ND7 treatment significantly reduced the microgliosis (Fig. 6 *G* and *H*) and astrogliosis (Fig. 6 *I* and *J*) in various brain regions by IHC staining of corresponding markers, Iba1 and GFAP, respectively (Fig. 6 *G–J*). Interestingly, imiglucerase treatment also reduced the Iba1 signal in the cortex compared with PBS treated group. We conclude that imiglucerase treatment significantly inhibited inflammation in visceral organs (*SI Appendix*, Fig. S14), which in turn results in reduced infiltration of inflammatory cells to CNS indirectly. TMEM119, another specific microglia marker (42), was used to confirm the alleviation of microgliosis in the brain. As expected, ND7 treatment significantly suppressed TMEM119 expression in both midbrain and cortex compared to PBS and imiglucerase-treated groups (*SI Appendix*, Fig. S15). Compared with reduced Iba1 level in cortex,

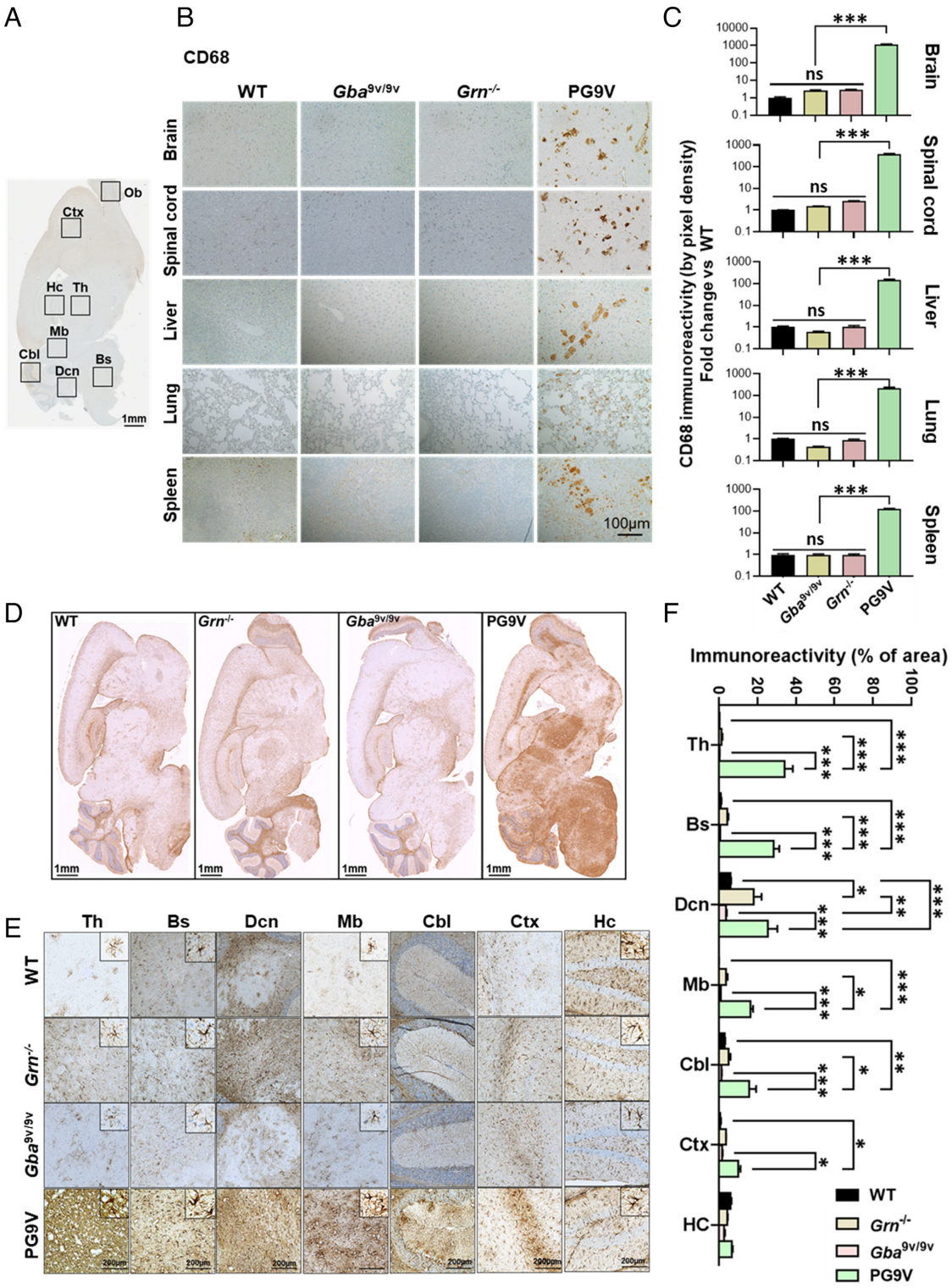

Fig. 5. PGRN deficiency led to hyperactivation of macrophages and astrocytes in PG9V mice. (*A*) Schematic diagram showing brain regions/areas of interest immunohistochemistry (IHC) quantitation. Ob, olfactory bulb; Ctx, cortex; Hc, hippocampus; Th, thalamus; Mb, midbrain; Cbl, cerebellum; Dcn, deep cerebellar nuclei. Bs, brainstem. (*B*) IHC staining with anti-CD68 antibody (brown) on CNS (brain and spinal cord) and visceral organs (liver, lung, and spleen) sections from 12-mo-old WT, *Gba*$^{9v/9v}$, *Grn*$^{-/-}$, and PG9V mice. (*C*) Quantification of CD68 immunoreactivity in *B* by pixel density. (*D*) Astrogliosis in CNS was shown by IHC staining of GFAP (brown) on 12-mo-old PG9V mice brain tissues. (*E*) Representative images showing GFAP signal distribution in different regions of the brain tissues. Selected astrocytic morphology in each genotype was enlarged and shown in *Insets* on the upright corn of the adherent images. The sections were counter-stained with hematoxylin on cell nuclei. (*F*) Quantification analysis of GFAP immunoreactivity in (*E*). Data are shown as mean ± SD. One-way ANOVA tests. *$P < 0.05$; **$P < 0.01$; ***$P < 0.001$.

imiglucerase did not change the TMEM119 level in the cortex compared with PBS group. Iba1 was used as a marker for both macrophage and microglia, while TEME119 was a microglia-specific marker, the data further indicated that imiglucerase might affect the visceral macrophage activation but not for microglia activation in CNS. Moreover, treatment with ND7, but not PBS and imiglucerase, effectively prevented the accumulation of α-Syn and TDP-43 in the brain tissue (*SI Appendix*, Fig. S16 *A–D*).

In addition to $Gba^{9v/null}$ and PG9V animal models, the neuroprotective effects of ND7 were tested in the immortalized GD neuronal cells derived from *Gba1* knockout mice ($Gba^{-/-}$) (54, 55). Interestingly, PGRN level was significantly reduced in $Gba^{-/-}$ neurons compared to normal control $Gba^{+/+}$ neurons (*SI Appendix*, Fig. S17 *A* and *B*). Western blot and the immunofluorescence staining revealed that the expression level of TDP-43 was comparable between $Gba^{+/+}$ and $Gba^{-/-}$ neurons (*SI Appendix*, Fig. S17*C*); however, Tau was accumulated significantly in $Gba^{-/-}$ neurons (*SI Appendix*, Fig. S17 *D–F*). Upon ND7 treatment, Tau accumulation was remarkably reduced in mouse $Gba^{-/-}$ neurons, although to a lesser degree compared to imiglucerase (*SI Appendix*, Fig. S17 *G* and *H*). In addition, expression of ND7 and PGRN $Gba^{-/-}$ neurons transfected by green fluorescent protein (GFP) fused-ND7 or -PGRN plasmid could prevent Tau accumulation (*SI Appendix*, Fig. S17*I*).

ND7 Effectively Ameliorated the GD Phenotype in GD Patient-Derived Fibroblasts. To investigate if the anti-GD role of ND7 found in mouse model can be translated to human, the therapeutic effects of ND7 were evaluated in GD patient-derived fibroblasts (*SI Appendix*, Fig. S18). For this purpose, we generated PGRN deficient $GBA^{L444P/L444P}$ (L444P/$GRN^{-/-}$) fibroblasts by knockout *GRN* via CRISP-Cas9 technology in $GBA1^{L444P/L444P}$ (L444P) fibroblast (*SI Appendix*, Fig. S18*A*). Loss of GRN in L444P/$GRN^{-/-}$ cells was confirmed by western blot (*SI Appendix*, Fig. S18*B*). As parallel control to ND7, we expressed the recombinant full-length PGRN protein with His tag (*SI Appendix*, Fig. S18*C*) and characterized its purity and size by Coomassie blue staining (*SI Appendix*, Fig. S18*C*, *Left*) and western blot with anti-PGRN antibody (*SI Appendix*, Fig. S18*C*, *Right*). Compared to GD type 2 patient fibroblasts having $GBA1^{L444P/L444P}$ (L444P), L444P/$GRN^{-/-}$ fibroblasts displayed dysregulated lysosomal function, evidenced by elevated LysoTracker Red signals, indicative of more lysosomal storage contents than L444P fibroblasts (*SI Appendix*, Fig. S18 *D-F*). Upon recombinant PGRN and ND7 treatment, lysosomal storage contents were significantly reduced in L444P/$GRN^{-/-}$ cells (*SI Appendix*, Fig. S18 *D-F*). Additionally, the deletion of PGRN in L444P cells decreased GCase activity and protein levels, whereas ND7 and PGRN restored the activity and GCase protein levels in L444P/$GRN^{-/-}$ cells (*SI Appendix*, Fig. S18 *G-I*). Furthermore, the therapeutic effects of ND7 and PGRN on GluCer accumulation were assayed using co-staining with anti-GluCer antibody and anti-lysosomal-associated membrane protein 1 (LAMP1) antibody (*SI Appendix*, Fig. S18*J*). PGRN deficiency increased, whereas recombinant ND7 or PGRN reduced GluCer accumulation in L444P cells (*SI Appendix*, Fig. S18*K*). To determine whether ND7 treatment is also effective for other *GBA1* mutations, recombinant PGRN and ND7 were further tested in type 1 GD patient fibroblasts with $GBA1^{N370S/84GG}$(N370S) mutation. Both ND7 and PGRN treatment decreased the lysosomal storage and GluCer accumulation and increased GCase activity (*SI Appendix*, Fig. S19). Although PGRN showed similar therapeutic effects against GD as ND7, because multifunctional PGRN may cause adverse effects, including potential oncogenic activity, therefore, we conclude that ND7, but not PGRN, holds a promise as a drug candidate in treating GD and PD.

Discussion

In our previous studies, we found that PGRN interacts with GCase (encoded by *Gba1*) and enhances GCase activity (20). PGRN is important for the lysosomal appearance of GCase, its deficiency leads to GCase aggregation in the cytoplasm, and the loss of PGRN dysregulates GCase folding and intracellular transportation and leads to GD-like phenotype in ovalbumin challenged $Grn^{-/-}$ mice (24). The current study is to determine the association of PGRN and mutant GCase, exemplified by $Gba^{9v/9v}$ (*Gba1* mutation in D409V). PGRN deficiency exacerbated the GD phenotypes and accelerated the onset and progression of GD, providing first direct in vivo evidence demonstrating the novel important role of PGRN in *GBA1* mutation-caused diseases. In addition, PGRN deficiency also worsened GD phenotypes in GD patient fibroblasts bearing various *GBA1* mutations (L444P and N370S), further confirmed the important role of PGRN in *GBA1* mutation-associated human GD phenotypes. Furthermore, bis(monoacylglycero)phosphate (BMP), an in vivo enhancer of lysosomal GCase activity, was decreased in $Grn^{-/-}$ mice (56), indicating that $Grn^{-/-}$ might have at least two direct effects on GCase—the delivery to the lysosome and the activation within the lysosome.

GBA1 mutations not only cause GD, but also are identified as the most common genetic risk factor for PD (27, 57). About 5 to 10% of the PD patients are heterozygous carriers for *GBA1* mutations (58). A roadblock in studying *GBA1* mutation-associated diseases, including nGD and PD, is the absence of animal models that recapitulate the disease pathobiology in multiple organs in humans. The developed *Gba1* mutant mouse models had limitations. Analogue models of human GD were developed by knocking in *Gba1* mutations homozygous for D409H, D409V, V394L, or L444P (9, 59), which are common mutations identified in GD patients (3, 60). Disappointedly, these mice do not develop considerable substrate accumulation and inflammation to cause clearly detectable or very minor disease phenotypes in viscera, and their nGD phenotypes vary from normal to mild (9, 61). The chronic nGD mouse models (9H/PS-NA and 4L/PS-NA) have combinations of *Gba1* mutations (D409H, 9H; V394L, 4L) with partial deficiency of prosaposin (62). Prosaposin encodes saposins (sphingolipid activator proteins) A, B, C, and D, which are lysosomal glycoproteins that are essential to the optimal activity of glycosphingolipid hydrolases, including GCase (63). These models displayed systematic GluCer accumulation and developed a more severe GD phenotype than mice with specific point mutations alone. However, loss of saposins potentially affects other glycosphingolipid hydrolases, which may result in mixed disease phenotype that are difficult to characterize. In addition, a nGD mouse model by combing the *Gba1* homozygous mutation for V394L with saposin C deficiency does not develop visceral disease—due to their short life span (64). In contrast to previously developed mouse models, PG9V mouse model through crossing $Grn^{-/-}$ and $Gba^{9v/9v}$ resulted in rapid progression of substrates (GluCer and GluSph) accumulation and inflammation in viscera (lung, liver) and CNS (brain, spinal cord) to the levels remarkably higher than those in $Grn^{-/-}$ and $Gba^{9v/9v}$ mice. They developed abnormal behavior, aggregation of neurodegenerative markers, hyperactivated microglia and astrocytes, indicating that PG9V mice exhibited neurodegenerative pathology. Importantly, the brain tissue of PG9V mice showed typical nGD phenotypes, which were not all present in $Gba^{9v/9v}$ mice, suggesting PG9V mice could serve as a novel candidate model of nGD. In addition, PG9V mice model is similar to the partial deficiency of PGRN that occurs in GD patients (20). As a co-chaperone of Hsp70, PGRN directly binds to GCase, helping GCase trafficking and lysosomal localization. The deficiency of PGRN in $Gba^{9v/9v}$ mice might lead to lower amounts of GCase being delivered to lysosomes and affect GCase stabilization as well. Moreover, $Grn^{-/-}$ mice led to deficiency of BMP, an essential anionic lipid that is vital for GCase activity (56). In PG9V mice, the absence of PGRN in lysosome might lead to an intralysosomal deficiency of BMP

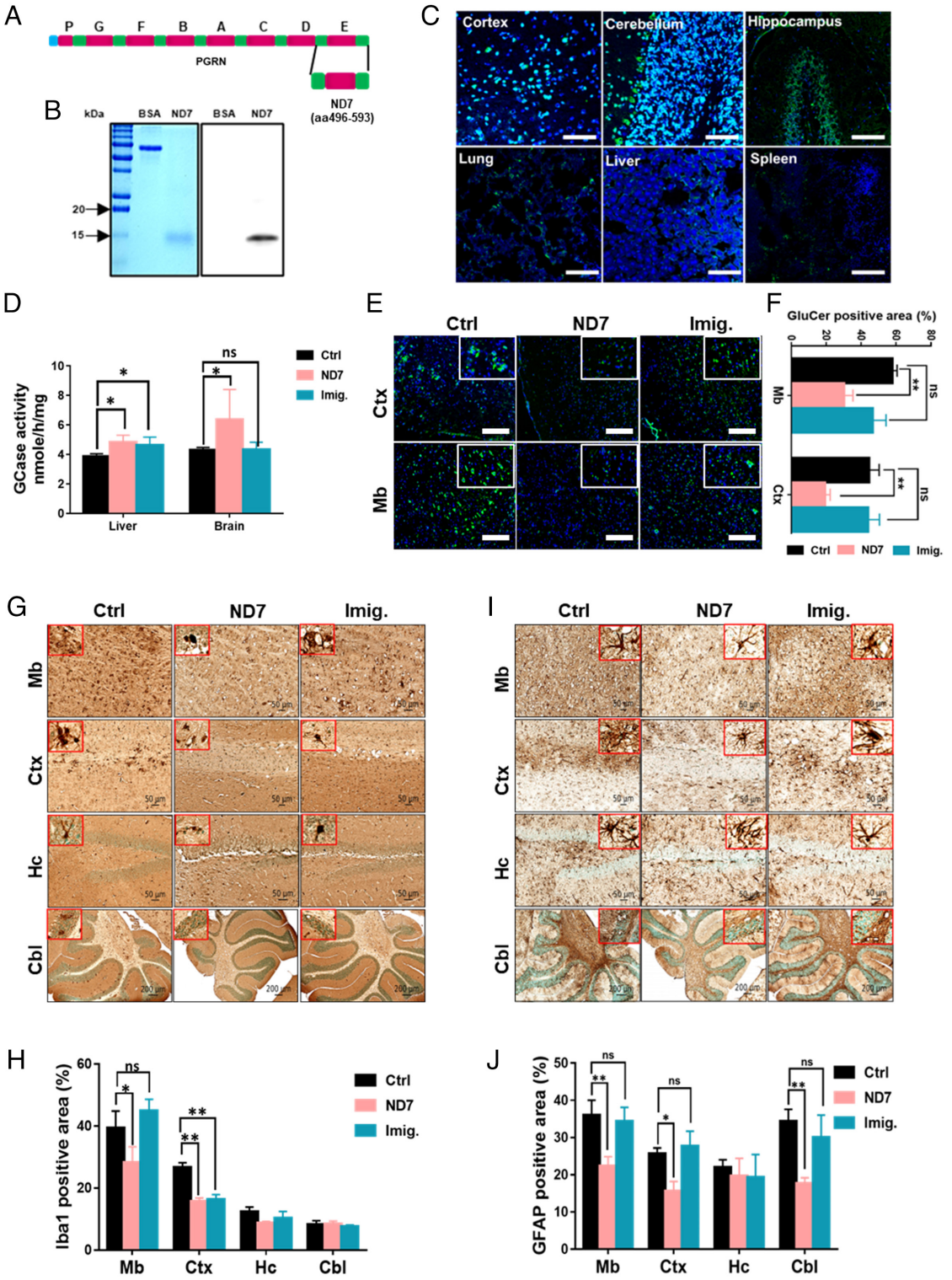

Fig. 6. PGRN derivative ND7 protected against GD phenotypes of PG9V mice. (*A*) Diagram of PGRN and ND7. ND7 (the seventh N-terminal deletion) is derived from C-terminal human PGRN from aa496-593, containing Grn E and linker regions on both sides. PGRN regions were highlighted in red, which include seven and half functional domain (P, G, F, B, A, C, D, E). The full-length linker regions are highlighted in green. Half-length region linker 5′ to domain P is highlighted in blue. (*B*) Expression and characterization of recombinant His-tagged ND7. Purified ND7 was analyzed by Coomassie blue staining (*Left*) and western blotting with anti-PGRN antibody (*Right*). BSA is a negative control. (*C*) Tissue distribution of His-tagged ND7. ND7 conjugated His-tag signals (green) were detected by anti-His-tag antibody in brain and visceral tissues from *Gba*$^{9v/null}$ mice administrated with 16 mg ND7/kg body weight (30 min post-injection). Representative images were shown. DAPI stained nuclei. (*D*) GCase activity in liver and brain from PBS, ND7, or imiglucerase (Imig.)-treated PG9V mice (24 h post last injection). (*E*) GluCer levels in brain from control, ND7-, or Imig-treated PG9V mice were determined using immunofluorescence staining with anti-GluCer antibody. (*F*) Quantification analysis of GluCer levels from *E*. (*G* and *I*) Activation of microglia and astrocytes in brain regions from control, ND7-, or Imig-treated PG9V mice were measured using IHC staining with antibody against Iba1 (*G*) and GFAP (*I*), respectively. (*H* and *J*) Quantification analysis of Iba1 (*G*) and GFAP (*I*) immunoreactivities. Mb, midbrain; Ctx, cortex; Hc, hippocampus; Cbl, cerebellum. Data are shown as mean ± SD. One-way ANOVA tests. *$P < 0.05$; **$P < 0.01$; ns, no significance. (Scale bar, 100 μm.)

which may directly cause or potentiate accumulation of GCase substrates. PGRN was reported to be involved in PD (18). It is equally important that PG9V mice also developed PD-like phenotypes, as manifested by the remarkable aggregation and accumulation of PD pathogenic markers, α-Syn and β-Amyloid, in the brain. Collectively, the PG9V mouse model overcomes the barriers to allow the study of *GBA1* mutation-caused diseases in multiple organs in viscera and CNS and provides a model faithfully resembling GD and PD for preclinical studies.

Inflammation and altered immunity play important roles in the pathogenesis of GD. PGRN acts as an anti-inflammation molecule by direct biding to tumor necrosis factor (TNF) receptors (15), and the deficiency of PGRN enhances macrophage-mediated inflammation in the brain tissue (40). In this study, tubular-like lysosomes were mainly presented in the macrophages, and there was stronger macrophage activation in visceral organs of PG9V mice, along with increased activation of microglia and astrocytes in the brain in PG9V mice than other controls, suggesting that PGRN deletion potentiated inflammation in *Gba1* mutant mice. In addition, PGRN deficiency markedly enhanced pro-inflammatory M1 macrophage polarization, while simultaneously inhibited anti-inflammatory M2 macrophage polarization in both $Grn^{-/-}$ and PG9V mice, compared with WT and $Gba^{9v/9v}$ mice. These results suggested that the PGRN deletion contributed to enhancing inflammation through, at least in part, modulating macrophage polarization.

Currently, ERT is mainly available as an effective treatment for non-neuropathic type 1 GD in clinics. ERT offsets low levels of GCase enzyme with a modified version of the enzyme. However, ERT is very expensive (around $350,000/y/patient) and not effective for all patients (3, 65, 66). In addition, the recombinant enzyme in ERT cannot penetrate the BBB and is ineffective for treating the primary CNS disease of neuropathic GD, i.e., types 2 and 3 GD. Approved SRT drugs have shown similar clinical improvement in visceral disease parameters but have no therapeutic utility for neuropathic GD (67–69). Thus, developing an alternative treatment for GD, specifically for nGD, is an urgent and unmet medical need. Some small molecule showed BBB penetration activity and therapeutic effect for treating GD, such as Ambroxol, treating patients with PD both with and without *GBA1* gene mutations (70). However, Ambroxol targets multiple biological process and pathways, which make it very challenging to control off-target effects in treating GD (71–74). On the other hand, neuroprotective role with beneficial drug concentration of Ambroxol in CNS can only be achieved at very high dose by oral administration (75), which may result in potential toxicity to other organs. In addition, Ambroxol is a pH-dependent inhibitor of GCase (71, 76) and its effect depends on the genotype for selected mutations (75, 77). In comparison, ND7 is a brain penetrant derivative of a native protein PGRN with clear mechanism of selectively increasing GCase activity through acting as a co-chaperone with Hsp70 and assisting GCase trafficking and lysosomal localization (24). ND7 is a biological function domain of PGRN without oncogenic activity, and long-term treatment of ND7 did not show toxicity in animals (*SI Appendix*, Fig. S20). Herein, ND7's therapeutic effects were tested in several in vivo and ex vivo models, including $Gba^{9v/null}$ and PG9V mice, mouse $Gba^{-/-}$ neurons, and GD patient fibroblasts. The present data revealed that ND7 crosses the BBB, penetrates into the brain parenchyma, significantly increases the GCase activity, and decreases the accumulation of the substrate GluCer in the brain tissue. In contrast, imiglucerase, a recombinant GCase used for treating GD type 1, non-neuropathic patients, did not cross BBB to show any primary CNS effects, although both ND7 and imiglucerase alfa effectively reduced the accumulation of substrate GluCer in the visceral organs. Additionally, ND7 showed anti-inflammation activity including reduced macrophage-mediated inflammation in lung and liver, as well as reduced microglia and astrocyte activity in brain which was not seen in imiglucerase-treated mice. These findings further support the CNS distribution and efficacy of ND7. Aside from ameliorating GD phenotype, ND7 treatment prevents the accumulation of widely used markers for neurodegenerative diseases, Tau, TDP-43, and α-Syn, supporting a promising therapeutic potential of ND7 for treating PD and other neurodegenerative diseases. In addition, ND7 could also ameliorate GD phenotypes in different mutant GCases found in type 1 and type 2 patients, evidenced by enhancement of GCase and reduction of lysosomal content and substrate levels (*SI Appendix*, Figs. S18, S19).

The evidence presented in the present study demonstrated that deletion of PGRN in $Gba^{9v/9v}$ mice potentiated systematic inflammation and typical GD and PD phenotypes which were not observed in either isolated $Grn^{-/-}$ or $Gba^{9v/9v}$ mice. However, each individual mutation of *GBA1* may have different influence on altering GCase protein three-dimensional structure, which is of important in forming the active catalytic pocket for its substrates. Therefore, the interaction between PGRN with other *GBA1* mutations (e.g., V394L and D409H) and the function of PGRN in other *Gba1* mutation-associated diseases need further investigation.

In summary, PGRN deficiency in *Gba1* mutant mice caused early onset and exacerbated GD phenotypes, leading to substantial increases in substrate accumulation and inflammation in visceral organs and CNS. Moreover, PG9V mice developed neurodegenerative manifestations of nGD and PD, including inflammation, neurodegeneration, and aggregation of neurodegenerative markers in the brain. Similarly, PGRN deficiency also worsened GD phenotypes in GD patient fibroblasts. These in vivo and ex vivo data demonstrated that PGRN plays a crucial role in the initiation, progression, and regulation of *GBA1* mutation-associated GD, providing a foundation for future studies related to this critical factor in GD and other LSDs. In addition, the PG9V mouse model overcomes many of the limitations of existing models, enables the studies of *GBA1* mutation-caused diseases and provides a clinical-relevant model system for testing therapeutic approaches for GD and PD. The unexpected findings that PGRN derivative ND7 crosses the BBB and protects against GD and PD-like pathology support a strong case for testing this reagent in a clinical trial.

Materials and Methods

Provided in the *SI Appendix, Materials and Methods*.

Data, Materials, and Software Availability. All study data are included in the article and/or *SI Appendix*.

ACKNOWLEDGMENTS. We would like to acknowledge all lab members for insightful discussions and critical reading. We thank Dr. Ellen Sidransky for providing mouse $Gba^{-/-}$ and $Gba^{+/+}$ neurons. We also thank Dr. Fengxia Liang at NYU Medical School OCS Microscopy Core for their assistance with confocal and electron microscope imaging. This work is supported partly by NIH research grants R01NS103931, R01AR062207, R01AR061484, R01AR076900, R01AR078035, R21OD033660, and a research grant from Atreaon.

Author affiliations: [a]Department of Orthopaedic Surgery, New York University Grossman School of Medicine, New York, NY 10003; [b]The Division of Human Genetics, Cincinnati Children's Hospital Medical Center, Cincinnati, OH 45229; [c]The Division of Pathology, Cincinnati Children's Hospital Medical Center, Cincinnati, OH 45229; [d]Department of Pediatrics, University of Cincinnati College of Medicine, Cincinnati, OH 45229; and [e]Department of Cell Biology, New York University Grossman School of Medicine, New York, NY 10016

1. F. M. Platt, Sphingolipid lysosomal storage disorders. *Nature* **510**, 68–75 (2014).
2. G. A. Grabowski, A. Zimran, H. Ida, Gaucher disease types 1 and 3: Phenotypic characterization of large populations from the ICGG Gaucher Registry. *Am. J. Hematol.* **90** (suppl. 1), S12–S18 (2015).
3. T. A. Burrow *et al.*, CNS, lung, and lymph node involvement in Gaucher disease type 3 after 11 years of therapy: Clinical, histopathologic, and biochemical findings. *Mol. Genet. Metab.* **114**, 233–241 (2015).
4. K. Reissner *et al.*, Type 2 Gaucher disease with hydrops fetalis in an Ashkenazi Jewish family resulting from a novel recombinant allele and a rare splice junction mutation in the glucocerebrosidase locus. *Mol. Genet. Metab.* **63**, 281–288 (1998).
5. J. Marshall *et al.*, Improved management of lysosomal glucosylceramide levels in a mouse model of type 1 Gaucher disease using enzyme and substrate reduction therapy. *J. Inherit. Metab. Dis.* **33**, 281–289 (2010).
6. J. Stirnemann *et al.*, A review of Gaucher disease pathophysiology, clinical presentation and treatments. *Int. J. Mol. Sci.* **18**, 441 (2017).
7. J. A. Shayman, Thematic review series: Recent advances in the treatment of lysosomal storage diseases. *J. Lipid Res.* **55**, 993–994 (2014).
8. G. A. Grabowski *et al.*, Gaucher disease: Basic and translational science needs for more complete therapy and management. *Mol. Genet. Metab.* **132**, 59–75 (2021).
9. Y. H. Xu *et al.*, Viable mouse models of acid beta-glucosidase deficiency: The defect in Gaucher disease. *Am. J. Pathol.* **163**, 2093–2101 (2003).
10. T. Farfel-Becker, E. B. Vitner, A. H. Futerman, Animal models for Gaucher disease research. *Dis. Model. Mech.* **4**, 746–752 (2011).
11. Y. Sun *et al.*, Gaucher disease mouse models: Point mutations at the acid beta-glucosidase locus combined with low-level prosaposin expression lead to disease variants. *J. Lipid Res.* **46**, 2102–2113 (2005).
12. J. Jian *et al.*, Progranulin: A key player in autoimmune diseases. *Cytokine* **101**, 48–55 (2018).
13. A. Bateman, H. P. Bennett, The granulin gene family: From cancer to dementia. *Bioessays* **31**, 1245–1254 (2009).
14. Z. He *et al.*, Progranulin is a mediator of the wound response. *Nat. Med.* **9**, 225–229 (2003).
15. W. Tang *et al.*, The growth factor progranulin binds to TNF receptors and is therapeutic against inflammatory arthritis in mice. *Science* **332**, 478–484 (2011).
16. J. S. Snowden *et al.*, Progranulin gene mutations associated with frontotemporal dementia and progressive non-fluent aphasia. *Brain* **129**, 3091–3102 (2006).
17. B. P. Chitramuthu, H. P. J. Bennett, A. Bateman, Progranulin: A new avenue towards the understanding and treatment of neurodegenerative disease. *Brain* **140**, 3081–3104 (2017).
18. N. Tayebi *et al.*, Pro-cathepsin D, prosaposin, and progranulin: Lysosomal networks in parkinsonism. *Trends Mol. Med.* **26**, 913–923 (2020).
19. K. R. Smith *et al.*, Strikingly different clinicopathological phenotypes determined by progranulin-mutation dosage. *Am. J. Hum. Genet.* **90**, 1102–1107 (2012).
20. J. Jian *et al.*, Association between progranulin and gaucher disease. *EBioMedicine* **11**, 127–137 (2016).
21. Y. Chen *et al.*, Progranulin associates with hexosaminidase A and ameliorates GM2 ganglioside accumulation and lysosomal storage in Tay-Sachs disease. *J. Mol. Med. (Berl.)* **96**, 1359–1373 (2018).
22. J. Jian, A. Hettinghouse, C. J. Liu, Progranulin acts as a shared chaperone and regulates multiple lysosomal enzymes. *Genes Dis.* **4**, 125–126 (2017).
23. M. E. Ward *et al.*, Individuals with progranulin haploinsufficiency exhibit features of neuronal ceroid lipofuscinosis. *Sci. Transl. Med.* **9**, eaah5642 (2017).
24. J. Jian *et al.*, Progranulin recruits HSP70 to beta-glucocerebrosidase and is therapeutic against Gaucher disease. *EBioMedicine* **13**, 212–224 (2016).
25. Y. Cui, A. Hettinghouse, C. J. Liu, Progranulin: A conductor of receptors orchestra, a chaperone of lysosomal enzymes and a therapeutic target for multiple diseases. *Cytokine Growth Factor Rev.* **45**, 53–64 (2019).
26. A. W. Kao *et al.*, Progranulin, lysosomal regulation and neurodegenerative disease. *Nat. Rev. Neurosci.* **18**, 325–333 (2017).
27. L. F. Burbulla *et al.*, A modulator of wild-type glucocerebrosidase improves pathogenic phenotypes in dopaminergic neuronal models of Parkinson's disease. *Sci. Transl. Med.* **11**, eaau6870 (2019).
28. Z. Ahmed *et al.*, Accelerated lipofuscinosis and ubiquitination in granulin knockout mice suggest a role for progranulin in successful aging. *Am. J. Pathol.* **177**, 311–324 (2010).
29. X. Zhao *et al.*, Progranulin associates with Rab2 and is involved in autophagosome-lysosome fusion in Gaucher disease. *J. Mol. Med. (Berl.)* **99**, 1639–1654 (2021).
30. Y. Sun *et al.*, Substrate compositional variation with tissue/region and Gba1 mutations in mouse models–Implications for Gaucher disease. *PLoS One* **8**, e57560 (2013).
31. A. Mendsaikhan, I. Tooyama, D. G. Walker, Microglial progranulin: Involvement in Alzheimer's disease and neurodegenerative diseases. *Cells* **8**, 230 (2019).
32. D. C. Perry *et al.*, Progranulin mutations as risk factors for Alzheimer disease. *JAMA Neurol.* **70**, 774–778 (2013).
33. J. M. Van Kampen, D. Baranowski, D. G. Kay, Progranulin gene delivery protects dopaminergic neurons in a mouse model of Parkinson's disease. *PLoS One* **9**, e97032 (2014).
34. C. Soto, S. Pritzkow, Protein misfolding, aggregation, and conformational strains in neurodegenerative diseases. *Nat. Neurosci.* **21**, 1332–1340 (2018).
35. C. A. Ross, M. A. Poirier, Protein aggregation and neurodegenerative disease. *Nat. Med.* **10** (suppl.), S10–S17 (2004).
36. S. Arawaka *et al.*, Mechanisms underlying extensive Ser129-phosphorylation in alpha-synuclein aggregates. *Acta Neuropathol. Commun.* **5**, 48 (2017).
37. G. Pagano *et al.*, Age at onset and Parkinson disease phenotype. *Neurology* **86**, 1400–1407 (2016).
38. L. Essabar *et al.*, Gaucher's disease: Report of 11 cases with review of literature. *Pan Afr. Med. J.* **20**, 18 (2015).
39. M. K. Pandey *et al.*, Complement drives glucosylceramide accumulation and tissue inflammation in Gaucher disease. *Nature* **543**, 108–112 (2017).
40. X. Zhao *et al.*, Analysis of the biomarkers for neurodegenerative diseases in aged progranulin deficient mice. *Int. J. Mol. Sci.* **23**, 629 (2022).
41. R. A. Feldman, Microglia orchestrate neuroinflammation. *Elife* **11**, e81890 (2022).
42. S. Bohnert *et al.*, TMEM119 as a specific marker of microglia reaction in traumatic brain injury in postmortem examination. *Int. J. Legal Med.* **134**, 2167–2176 (2020).
43. F. Gonzalez Ibanez *et al.*, Immunofluorescence staining using IBA1 and TMEM119 for microglial density, morphology and peripheral myeloid cell infiltration analysis in mouse brain. *J. Vis. Exp.* **152**, e60510 (2019).
44. P. Smethurst *et al.*, The role of astrocytes in prion-like mechanisms of neurodegeneration. *Brain* **145**, 17–26 (2022).
45. H. D. E. Booth, W. D. Hirst, R. Wade-Martins, The role of astrocyte dysfunction in Parkinson's disease pathogenesis. *Trends Neurosci.* **40**, 358–370 (2017).
46. S. C. Funes *et al.*, Implications of macrophage polarization in autoimmunity. *Immunology* **154**, 186–195 (2018).
47. C. Atri, F. Z. Guerfali, D. Laouini, Role of human macrophage polarization in inflammation during infectious diseases. *Int. J. Mol. Sci.* **19**, 1801 (2018).
48. L. Liu *et al.*, Progranulin inhibits LPS-induced macrophage M1 polarization via NF-small ka, CyrillicB and MAPK pathways. *BMC Immunol.* **21**, 32 (2020).
49. W. Fu *et al.*, TNFR2/14-3-3epsilon signaling complex instructs macrophage plasticity in inflammation and autoimmunity. *J. Clin. Invest.* **131**, e144016 (2021).
50. P. P. Y. Lie *et al.*, Post-Golgi carriers, not lysosomes, confer lysosomal properties to pre-degradative organelles in normal and dystrophic axons. *Cell Rep.* **35**, 109034 (2021).
51. Y. Hou *et al.*, Ageing as a risk factor for neurodegenerative disease. *Nat. Rev. Neurol.* **15**, 565–581 (2019).
52. A. Moreno-Garcia *et al.*, An overview of the role of lipofuscin in age-related neurodegeneration. *Front Neurosci.* **12**, 464 (2018).
53. F. Arechavaleta-Velasco *et al.*, Progranulin and its biological effects in cancer. *Med. Oncol.* **34**, 194 (2017).
54. W. Westbroek *et al.*, A new glucocerebrosidase-deficient neuronal cell model provides a tool to probe pathophysiology and therapeutics for Gaucher disease. *Dis. Model. Mech.* **9**, 769–778 (2016).
55. Y. Peng *et al.*, Substrate reduction therapy reverses mitochondrial, mTOR, and autophagy alterations in a cell model of Gaucher disease. *Cells* **10**, 2286 (2021).
56. T. Logan *et al.*, Rescue of a lysosomal storage disorder caused by Grn loss of function with a brain penetrant progranulin biologic. *Cell* **184**, 4651–4668.e25 (2021).
57. T. Farfel-Becker *et al.*, Can GBA1-associated Parkinson disease be modeled in the mouse? *Trends Neurosci.* **42**, 631–643 (2019).
58. E. Sidransky *et al.*, Multicenter analysis of glucocerebrosidase mutations in Parkinson's disease. *N. Engl. J. Med.* **361**, 1651–1661 (2009).
59. E. I. Ginns *et al.*, Neuroinflammation and alpha-synuclein accumulation in response to glucocerebrosidase deficiency are accompanied by synaptic dysfunction. *Mol. Genet. Metab.* **111**, 152–162 (2014).
60. G. A. Grabowski, G. A. Petsko, E. H. Kolodny, "Gaucher disease" in *The Online Metabolic and Molecular Bases of Inherited Diseases*, D. Valle *et al.*, Eds. (The McGraw-Hill Companies Inc., New York, 2010).
61. S. P. Sardi *et al.*, CNS expression of glucocerebrosidase corrects alpha-synuclein pathology and memory in a mouse model of Gaucher-related synucleinopathy. *Proc. Natl. Acad. Sci. U.S.A.* **108**, 12101–12106 (2011).
62. Y. Sun *et al.*, Gaucher disease mouse models: Point mutations at the acid beta-glucosidase locus combined with low-level prosaposin expression lead to disease variants. *J Lipid Res.* **46**, 2102–2113 (2005).
63. H. Schulze, T. Kolter, K. Sandhoff, Principles of lysosomal membrane degradation: Cellular topology and biochemistry of lysosomal lipid degradation. *Biochim. Biophys. Acta* **1793**, 674–683 (2009).
64. Y. Sun *et al.*, Neuronopathic Gaucher disease in the mouse: Viable combined selective saposin C deficiency and mutant glucocerebrosidase (V394L) mice with glucosylsphingosine and glucosylceramide accumulation and progressive neurological deficits. *Hum. Mol. Genet.* **19**, 1088–1097 (2010).
65. A. H. Futerman, F. M. Platt, The metabolism of glucocerebrosides–From 1965 to the present. *Mol. Genet. Metab.* **120**, 22–26 (2017).
66. T. Kirkegaard *et al.*, Heat shock protein-based therapy as a potential candidate for treating the sphingolipidoses. *Sci. Transl. Med.* **8**, 355ra118 (2016).
67. D. J. Kuter *et al.*, Miglustat therapy in type 1 Gaucher disease: Clinical and safety outcomes in a multicenter retrospective cohort study. *Blood Cells Mol. Dis.* **51**, 116–124 (2013).
68. E. Lukina *et al.*, Eliglustat, an investigational oral therapy for Gaucher disease type 1: Phase 2 trial results after 4 years of treatment. *Blood Cells Mol. Dis.* **53**, 274–276 (2014).
69. L. L. Bennett, D. Mohan, Gaucher disease and its treatment options. *Ann. Pharmacother.* **47**, 1182–1193 (2013).
70. S. Mullin *et al.*, Ambroxol for the treatment of patients with Parkinson disease with and without glucocerebrosidase gene mutations: A nonrandomized, noncontrolled trial. *JAMA Neurol.* **77**, 427–434 (2020).
71. A. McNeill *et al.*, Ambroxol improves lysosomal biochemistry in glucocerebrosidase mutation-linked Parkinson disease cells. *Brain* **137**, 1481–1495 (2014).
72. J. Magalhaes *et al.*, Effects of ambroxol on the autophagy-lysosome pathway and mitochondria in primary cortical neurons. *Sci. Rep.* **8**, 1385 (2018).
73. G. H. Maegawa *et al.*, Identification and characterization of ambroxol as an enzyme enhancement agent for Gaucher disease. *J. Biol. Chem.* **284**, 23502–23516 (2009).
74. T. Weiser, Ambroxol: A CNS drug? *CNS Neurosci. Ther.* **14**, 17–24 (2008).
75. A. Narita *et al.*, Ambroxol chaperone therapy for neuronopathic Gaucher disease: A pilot study. *Ann. Clin. Transl. Neurol.* **3**, 200–215 (2016).
76. A. Migdalska-Richards *et al.*, Ambroxol effects in glucocerebrosidase and alpha-synuclein transgenic mice. *Ann. Neurol.* **80**, 766–775 (2016).
77. B. Charkhand *et al.*, Effect of Ambroxol chaperone therapy on Glucosylsphingosine (Lyso-Gb1) levels in two Canadian patients with type 3 Gaucher disease. *Mol. Genet. Metab. Rep.* **20**, 100476 (2019).